Optical absorption and exciton linewidths of $Zn_{1-x}Cd_xSe$ quantum wells

P. M. Young, E. Runge, M. Ziegler, and H. Ehrenreich
Division of Applied Sciences, Harvard University, Cambridge, Massachusetts 02138
(Received 12 July 1993; revised manuscript received 19 October 1993)

Comparison of experimentally determined optical spectra of $Zn_{1-x}Cd_xSe/ZnSe$ quantum wells with theoretical results for fundamental optical absorption and exciton linewidths is used to determine valence-band offset and properties of exciton features as a function of well width and temperature. The heavy-hole valence-band offset is found to be approximately 90 meV for $x=0.23$. The exciton linewidths are analyzed in terms of Gaussian inhomogeneous broadening attributable to expected sample inhomogeneities involving well widths and alloy concentrations and homogeneous broadening associated with exciton-optical-phonon interactions. The linewidths are found to be smaller and larger than the bulk value for narrow (30 Å) and wide (200 Å) widths, respectively, in agreement with experimental results.

I. INTRODUCTION

This theoretical study of the optical spectra of $Zn_{1-x}Cd_xSe/ZnSe$ quantum wells (QW's) analyzes experimentally determined fundamental optical absorption to (1) interpret exciton features, (2) deduce valence-band offsets, and (3) determine the well width and temperature dependence of the exciton linewidths. To the best of our knowledge, this is the first time that the features of optical-absorption spectra for wide-gap II-VI heterostructures have been calculated in detail. The optical properties of this system are of technological importance because $Zn_{1-x}Cd_xSe/ZnSe$ QW's have been employed as the active region of the first experimentally demonstrated blue-green injection laser diodes.[1,2] This work represents an extension of techniques previously applied to the calculation of the optical properties of III-V heterostructures.[3-5] The agreement between experiment and theory is significantly diminished relative to that of the III-V systems. These shortcomings emphasize important qualitative differences between the III-V's and II-VI's which are also observed in the bulk materials, but frequently overlooked in the literature.

Calculations are based on a superlattice (SL) formalism,[6] which permits definition of a crystal momentum and use of crystal coordinate representations.[3] Our formalism has been presented elsewhere.[3-8] Previously unpublished generalizations that include the effects of strain in lattice mismatched systems are briefly described in the Appendix. The effects of the electron-hole Coulomb interaction are taken into account using a "rod" model potential[3-5] for which the exciton envelope functions are represented by uniformly charged rods, whose extent is roughly a SL cell. The quantitative validity of this approach for the cases of interest here has been tested previously.[4] The energies of QW exciton states and their optical properties may thus be calculated without resorting to a variational approach.

The overall structure of the optical spectra is considered in Sec. II. The various features seen in the experimental spectra[9] are calculated and unambiguously identified. Agreement with experimental results is obtained for a value of the valence-band offset of about 90 meV for the heavy-hole edge in $Zn_{0.77}Cd_{0.23}Se/ZnSe$ QW's. This result represents the first reasonably accurate determination of that offset based directly on experimental data. The linewidth of the lowest-lying exciton is examined in Sec. III. The large strength of the polar-optical interaction between carriers and longitudinal-optical (LO) phonons combined with the large exciton binding energies in these QW's results in a homogeneous exciton linewidth as a function of well width and temperature which is qualitatively different from that observed in other QW's studied to date.[10] A Gaussian contribution to the linewidth, attributable to experimentally reasonable sample inhomogeneities involving well widths and the alloy concentrations, is also calculated. This contribution dominates at low temperatures and is temperature independent. The homogeneous linewidths are found to be smaller than the bulk value for narrow 30-Å wells, but larger for wide 200-Å wells, in agreement with experiment. We believe that this work represents the first qualitative explanation of *both* of these unexpected experimental observations. The result is of interest since lasing may occur directly from the exciton states in this system.[11]

II. ABSORPTION SPECTRA

Optical-absorption spectra are calculated using the techniques of Ref. 4, with the effects of strain incorporated as discussed in the Appendix. The QW Wannier functions are localized to a volume which has in-plane dimensions comparable to the bulk lattice constant and a length comparable to the well width. This fact has suggested a rod model[3] in which the electron-hole Coulomb interaction is modeled by the potential of one-dimensional rods oriented along the growth direction and having charge $\pm e$. The independent subband approximation,[4,5,8] valid for wells with widths as wide as a few times the exciton Bohr radius, associates each exciton with a single conduction and single valence subband. As has been demon-

strated previously, exciton states and their optical absorption can be calculated both accurately and efficiently from the band structure using this model without resorting to a variational approach. The confinement of electron and hole states in the wells results in quasi-2D excitons which have larger binding energies and oscillator strengths relative to bulk values. The effects of the Sommerfeld enhancement of the optical absorption are also increased. This method has been used to obtain excellent agreement between theory and experiment for III-V heterostructures with exciton peak locations agreeing within 2–3 meV, and overall absorption strengths in absolute units within $\approx 10\%$.[4] The success of this approach has led to its employment as a tool to analyze defects in QW structures[12] and to determine valence-band offsets.[4]

Ding and co-workers[9,13] measured optical-absorption spectra for the three $Zn_{1-x}Cd_xSe$ QW samples considered here at 10 K. Each sample contains six wells separated by 500-Å ZnSe barriers. The wells have nominal concentrations of $x=0.25$ and widths of 30, 60, and 90 Å, respectively. The absolute optical absorption was roughly determined, but this was not a goal of the experimental work. Nevertheless, the current theoretical results for the absolute absorption strength agree reasonably well. They are approximately a factor of 2 lower than the experimental estimate, which is similar in magnitude to the discrepancy for bulk ZnSe. Together, these results illustrate the qualitative differences between the III-V's and II-VI's with respect to agreement between theory and experiment.

The $Zn_{1-x}Cd_xSe$ band gap and the splitting of the heavy and light holes are sensitive functions of x; the gap varies by about 10 meV and the splitting by about 3 meV per 1% change in x. Therefore the alloy concentrations used in the calculations were varied within the range of experimental uncertainty in order to obtain approximate agreement in the location of the *lowest* (and only the lowest) exciton peak. The experimentally observed linewidth of this lowest bound exciton together with the calculated oscillator strength are used to determine the peak absorption value. The entire experimental spectrum is then normalized to this peak value. The valence-band offset is used as a fitting parameter to obtain the best agreement between theory and experiment. The parameters used to perform the absorption calculations are summarized in Table I. For this system the bulk Bohr radius is about 40 Å. The independent subband approximation should hold over the range of wells under examination.

The resulting spectra are illustrated in Fig. 1 for (a) 30-Å, (b) 60-Å, and (c) 90-Å QW's. Note again that agreement between experiment and theory for the lowest exciton peak results from a three-parameter fit involving the overall strength, low-temperature linewidth, and (to some extent) energy. This procedure contrasts sharply with our previous work on the much better characterized III-V's where fitting parameters were not required.[4]

We emphasize that the fit to the lowest exciton peak does not affect the reliability of the valence-band-offset (Λ_{HH}) determination described below which depends only on the higher-order features that require no further adjustment. Table II shows the value determined here of $\Lambda_{HH}=90$–95 meV to be nearly the same for all three samples. Table II also summarizes the geometry and compositions (both nominal and theoretically required) for each sample.

TABLE I. A summary of the bulk **k·p** parameters, lattice constants, elastic parameters, and dielectric constants used in the present calculations. E_g is the fundamental gap, Δ is the spin-orbit splitting, m_{HH} is the heavy-hole mass, E_P is the energy associated with the Kane momentum matrix element, a is the lattice constant, C_{11} and C_{12} are elastic stiffness constants, c and b are hydrostatic and biaxial deformation potentials, respectively, and ϵ_0 and ϵ_∞ are static and high-frequency dielectric constants, respectively. For $Zn_{1-x}Cd_xSe$, all values are linearly interpolated except E_g, which is taken from Ref. 14.

Parameter	ZnSe	CdSe
E_g (eV)	2.82[a]	1.75[b]
Δ (eV)	0.43[a]	0.42[a]
m_{HH}/m	0.49[c]	0.49[d]
E_P (eV)	19.5[e]	19.5[d]
a (Å)	5.668	6.077[f]
C_{11} (10^{11} dyn/cm^2)	8.88[g]	6.67[h]
C_{12} (10^{11} dyn/cm^2)	5.27[g]	4.63[h]
c (eV)	−5.4[i]	−3.0[i]
b (eV)	−1.2[i]	−0.7[i]
ϵ_0	8.7[j]	8.7[d]
ϵ_∞	5.6[j]	5.6[d]

[a]Reference 15.
[b]Reference 14.
[c]Reference 16.
[d]Extrapolated from value for ZnSe.
[e]Deduced from conduction-band mass m_c^* of Ref. 17 using $m/m_c^* \approx (\frac{2}{3})E_P/E_g + (\frac{1}{3})E_P/(E_g+\Delta)$.
[f]Reference 18.
[g]Reference 19.
[h]Deduced from elastic constants of wurtzite CdSe using the method of Ref. 20.
[i]Reference 21.
[j]Reference 22.

In Fig. 1(a) the absorption spectrum of the 30-Å QW has only two strong exciton features. The lower-energy peak corresponds to the 1*s* exciton associated with the lowest conduction band $C1$ and the highest heavy-hole valence band HH1. The higher-energy peak corresponds to the 1*s* exciton associated with the highest light-hole band LH1 and $C1$. Both features are clearly resolved in the theoretical (solid line) and experimental (dashed line) spectra. Two addition features are seen in Fig. 1(b), which shows the spectra of the 60-Å sample. The first is the 1*s* exciton peak associated with the HH2-$C2$ subband

TABLE II. Summary of quantum-well geometries, nominal $Zn_{1-x}Cd_xSe$ alloy concentrations, and values yielding best fit to the locations of the lowest exciton peak and to the heavy-hole valence-band offset.

Well width (Å)	30	60	90
$x_{Nominal}$	25	25	24
x_{Fit}	22	22	24.5
Λ_{HH} (meV)	90	90	95

pair, and the second is the continuum edge associated with HH1-$C1$ transitions. The latter feature, however, is resolved only in the theoretical spectrum where it appears as a shoulder on the low-energy side of the LH1-$C1$ peak. The spectrum of the 90-Å sample shown in Fig. 1(c) exhibits the HH3-$C3$ exciton; however, the LH1-$C1$ and HH2-$C2$ excitons occur at the same excitation energy. Table III lists the energies and assignments of the observed exciton peaks. In all of the spectra experimental absorption increases more rapidly than theory with increasing photon energy. This effect may be attributed at least in part to Urbach tail absorption in the wide ZnSe layers present in the sample.

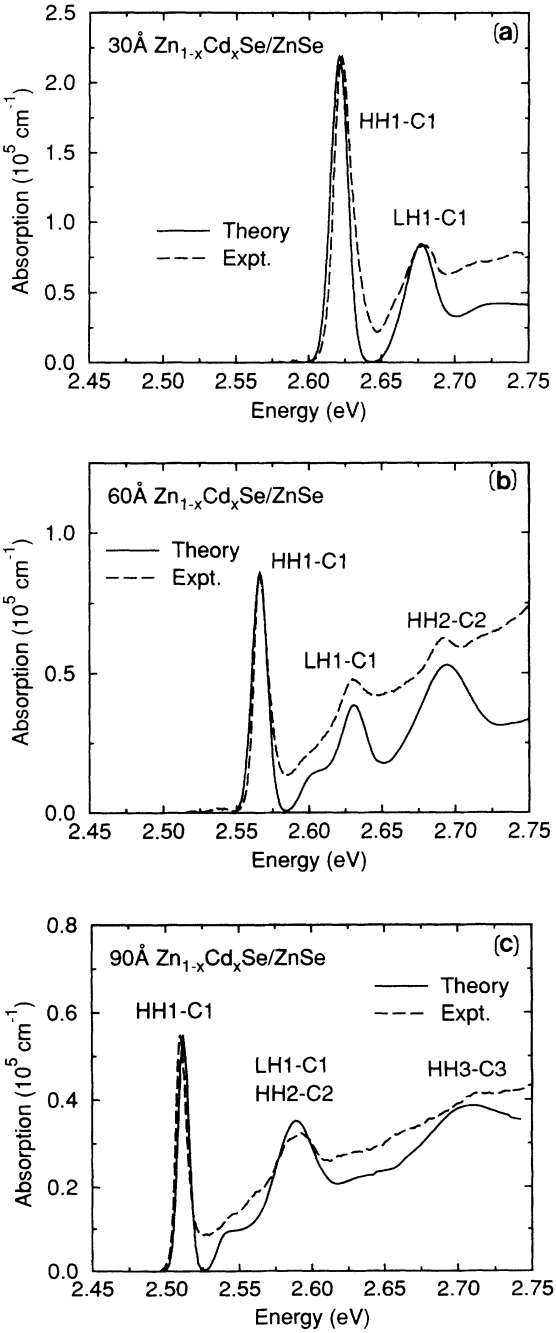

FIG. 1. Calculated (solid lines) and experimental (dashed lines) spectra for $Zn_{1-x}Cd_xSe/ZnSe$ quantum wells with widths of (a) 30, (b) 60, and (c) 90 Å. Absorption scale refers to calculated curves only, and assumes the width of the absorbing medium is the combined width of the wells in the sample. Experimental curves have been normalized to agree with theory at the HH1-$C1$ peak. Major exciton peaks are identified.

TABLE III. Identification of the exciton peaks appearing in the absorption spectra (cf. Fig. 1).

Well width (Å)	30	60	90
HH1-$C1$	2.622 eV	2.566 eV	2.510 eV
LH1-$C1$	2.678 eV	2.631 eV	2.589 eV
HH2-$C2$		2.692 eV	2.589 eV
HH3-$C3$			2.712 eV

For the three samples the best agreement between theory and experiment is obtained for $\Lambda_{HH} \approx 90$ meV, though fair agreement is obtained throughout the range 75 meV $\leq \Lambda_{HH} \leq$ 125 meV. This range is consistent with the value $\Lambda_{HH}=80$ meV which has been used by Jeon *et al.* in Ref. 2. It is somewhat larger than the value of $\Lambda_{HH}=55$ meV obtained in Refs. 10 and 13 using theoretical values of the deformation potentials and the assumption that the unstrained offset for $Zn_{1-x}Cd_xSe/ZnSe$ is similar to the experimentally determined value for lattice-matched $Zn_{1-x}Cd_xSe/Zn_{1-y}Mn_ySe$ interfaces. Note that roughly 40 meV of Λ_{HH} is due to the biaxial strain, implying an average hole band offset of $\Lambda=50$ meV which extrapolates to $\Lambda=220$ meV for the CdSe/ZnSe interface. The common anion rule therefore does not seem to apply in this system.[23]

Another argument favoring the present estimate of the lower bound of 75 meV on the valence-band offset, Λ_{HH}, is the following. The single most important feature determining the quality of the fit to the experimental spectra is the LH1-$C1$ exciton peak, since its oscillator strength and separation from the HH1-$C1$ peak are sensitive to the value of the valence-band offset. The position of the LH1-$C1$ exciton is determined by the light-hole offset Λ_{LH} which is 75 meV less than Λ_{HH} as a result of the biaxial strain. For negative values of Λ_{LH} the light holes would be confined to the barrier layers, which would lead to a substantial decrease in the LH1-$C1$ oscillator strength. Since this reduction is not consistent with the experimental spectra, the lower bound of $\Lambda_{HH}=75$ meV is reasonable.

III. EXCITON LINEWIDTHS

The onset of the fundamental absorption edge in $Zn_{1-x}Cd_xSe/ZnSe$ QW's is dominated by the large oscillator strength of the HH1-$C1$ 1s exciton. It has been suggested that lasing action in the ZnSe-based blue-green lasers occurs directly out of this state, and therefore that the gain coefficient depends upon the exciton linewidth.[11,24] This linewidth has two major components: a Gaussian contribution attributable to sample inhomogeneities in the well width and alloy concentration, and a homogeneous contribution due to lifetime broadening caused primarily by polar-optical exciton-phonon interactions. The inhomogeneous linewidth is roughly tem-

perature independent, dominating at low temperature, while the homogeneous linewidth, due to single LO-phonon absorption, is proportional to the thermal population of the LO-phonon modes.

Recent experimental work[10] has shown that for QW's the exciton-LO-phonon coupling, as inferred from the homogeneous linewidths, is smaller than that in bulk ZnSe for narrow 30-Å wells, yet unexpectedly larger than that in bulk ZnSe for wide 200-Å wells. A theoretical explanation of these results follows.

The behavior of the full width at half maximum can be written in the form[10]

$$\Gamma(L_W,T)=\Gamma_0(L_W)+\Gamma_{\rm LO}(L_W)(e^{\hbar\omega_{\rm LO}/k_BT}-1)^{-1}\ , \tag{1}$$

where Γ_0 is the inhomogeneous linewidth, and $\Gamma_{\rm LO}$ represents the homogeneous linewidth factor which is multiplied by the occupation of dispersionless LO-phonon modes with energy $\hbar\omega_{\rm LO}$ and occupation $n=(e^{\hbar\omega_{\rm LO}/k_BT}-1)^{-1}$. Both Γ_0 and $\Gamma_{\rm LO}$ are assumed to depend only on the QW width, L_W. Contributions to the exciton lifetime from other mechanisms, such as acoustic-phonon scattering, are neglected.[25]

The inhomogeneous linewidth broadening is estimated by assuming single-monolayer fluctuations[4] in L_W which leads to fluctuations of 8 meV in the exciton energy for a 30-Å QW. The 8-meV value is deduced from the difference in energy gaps among 27-, 30-, and 33-Å wells. Broadening due to concentration fluctuations[10,26] is estimated by assuming an exciton volume of $\pi a_B^2 L_W$ containing $N=\pi a_B^2 L_W/v_c$ cations, where a_B is the exciton Bohr radius and v_c is the bulk unit-cell volume. The fluctuation in the concentration x of a perfectly random alloy within each exciton volume is then $2\sqrt{(2\ln 2)x(1-x)/N}$. The resulting distribution of exciton energies produces a Gaussian line shape whose width is

$$\Gamma_{\rm Alloy}=2\sqrt{(2\ln 2)x(1-x)}\left[\frac{v_c}{\pi a_B^2 L_W}\right]^{1/2}\times(E_g^{\rm ZnSe}-E_g^{\rm CdSe})\approx 13\ \text{meV}\ . \tag{2}$$

The first factor describes the concentration fluctuation, and the last, involving the difference in the energy gaps of ZnSe and CdSe, $E_g^{\rm ZnSe}-E_g^{\rm CdSe}$, characterizes the scale over which the exciton energy varies. The random fluctuations due to well width and allow concentration add in quadrature to give a total inhomogeneous linewidth of 15 meV, which is in agreement with the observed 13-meV linewidth of 30-Å wells.[10]

The observed temperature dependence of the linewidth $\Gamma(L_W,T)$ is fit well by single LO-phonon absorption.[10] Applying the Fröhlich Hamiltonian, the lifetime broadening[27,28] $\Gamma_{\rm LO}=\hbar/\tau$ due to scattering of the 1s HH1-C1 exciton is given within the Born approximation by

$$\Gamma_{\rm LO}=\frac{4\pi^2\hbar\omega_{\rm LO}e^2}{\epsilon_p\Omega}\sum_q\sum_f\frac{1}{q^2}|\langle i|e^{i\mathbf{q}\cdot\mathbf{r}_e}-e^{i\mathbf{q}\cdot\mathbf{r}_h}|f\rangle|^2\times\delta(E_f-E_i-\hbar\omega_{\rm LO})\ , \tag{3}$$

where Ω is the sample volume, $\epsilon_p^{-1}=\epsilon_\infty^{-1}-\epsilon_0^{-1}$, where ϵ_∞ and ϵ_0 are the high-frequency and static dielectric constants, respectively, and the sums extend over the phonon mode wave vectors q and final exciton states f. The phonon modes are assumed to have the average bulk energy $\hbar\omega_{\rm LO}=31$ meV.[10] The exciton states are modeled using the independent subband approximation,[4] in which each exciton is associated with a single conduction band L and single valence band M. The electron and hole states are each described in terms of a single $\mathbf{K}$-independent envelope function, so that a separable form for the exciton state

$$\Psi(\mathbf{r}_e,\mathbf{r}_h)=F_L(z_e)F_M(z_h)\varphi(\rho)e^{i\mathbf{K}\cdot\mathbf{R}}\ , \tag{4}$$

is obtained. The conduction and valence subbands have parabolic bands of mass m_L^* and m_M^*, respectively, and the in-plane center-of-mass coordinate and the relative coordinate, respectively, are given by

$$\mathbf{R}=(m_L^*\mathbf{r}_e^{\parallel}+m_M^*\mathbf{r}_h^{\parallel})/(m_L^*+m_M^*)\ , \tag{5}$$

and

$$\rho=\mathbf{r}_e^{\parallel}-\mathbf{r}_h^{\parallel}\ . \tag{6}$$

The envelope functions are assumed to be those of the hard-wall QW, in which

$$F_n(z)=\left[\frac{2}{L_W}\right]^{1/2}\sin\left[\frac{n\pi}{L_W}z\right] \tag{7}$$

is nonvanishing only in the interval $0\le z\le L_W$; for example, $F_{C1}(z)=F_{\rm HH1}(z)=F_1(z)$. The exciton wave function in the relative coordinate $\varphi(\rho)$ is modeled by two-dimensional (2D) hydrogenic states. At large ρ these states fall off as $e^{-\sqrt{|E_{\rm 2D}|/R_H}(\rho/a_B)}$, where $R_H=e^2/2\epsilon_0 a_B$ is the exciton Rydberg, $a_B=\epsilon_0\hbar^2/\mu e^2$ is the exciton Bohr radius involving the reduced mass $\mu^{-1}=(m_L^*)^{-1}+(m_M^*)^{-1}$, and $E_{\rm 2D}=-R_H/(n-\frac{1}{2})^2$ where n is an integer. The finite width of real QW's increases the effective in-plane exciton radius and substantially decreases the exciton binding energies from these values. The effects of finite well width are accounted for in the present calculation by replacing a_B by $a_B\sqrt{E_{\rm 2D}/E_{\rm Rod}}$ in the form for the 2D wave functions. ($E_{\rm Rod}$ is the QW binding energy obtained from the rod model.)

The initial state, the HH1-C1 exciton at $\mathbf{K}=\mathbf{0}$, connects to a number of possible final states. The independent subband approximation employed here is valid only for $L_W\lesssim 3a_B$,[5] or about 120 Å. In this range the important available energy-conserving final states involving 31-meV phonon absorption are the HH1-C1 1s states with $\mathbf{K}\neq\mathbf{0}$, HH1-C1 2s and 2p states, and HH2-C1 1s states. More highly excited HH1-C1 bound exciton states, such as 3s, 3p, etc., are expected to be only weakly coupled to the HH1-C1 state in comparison to the 2s and 2p states, and are neglected.

After some calculation, similar to that involving LO-phonon absorption in SL electron transport,[27,28] Eq. (3) for $\Gamma_{\rm LO}$ can be conveniently expressed in the form

$$\Gamma_{\mathrm{LO}}=\sum_f \frac{1}{\epsilon_p}\hbar\omega_{\mathrm{LO}}\frac{me^2}{\hbar^2}\frac{M_{LM}}{m}\frac{\pi}{K_f}J_n(K_f) \times\left|\delta_{M,\mathrm{HH1}}I_f\left[\frac{m_M^*}{M_{LM}}K_f\right]-\delta_{L,C1}I_f\left[\frac{m_L^*}{M_{LM}}K_f\right]\right|^2, \tag{8}$$

which involves a product of integrals

$$J_n(Q)=\int\int dzdz' F_1(z)F_1(z')F_n(z)F_n(z')e^{-Q|z-z'|}, \tag{9}$$

representing the square of the overlap of the envelope functions (corresponding to HH1-$C1$ and HH2-$C1$ transitions for $n=1$, and 2, respectively) weighted by all phonons with in-plane momentum Q, and

$$I_f(\mathbf{k})=\int d^2\rho\,\varphi_{1s}(\rho)\varphi_f(\rho)e^{i\mathbf{k}\cdot\rho}, \tag{10}$$

representing the overlap of the initial and final exciton wave functions. Here K_f is the final state in-plane wave vector given by conservation of energy, $M_{LM}=m_L^*+m_M^*$ is the total exciton mass, and the sum over final states f extends over all L, M, and exciton wave functions φ_f.

Calculated results for $\Gamma_{\mathrm{LO}}(L_W)$ over the range 20 Å $\le L_W \le$ 120 Å are shown in Fig. 2 (solid curve), along with experimental results[10] (crosses) for $Zn_{0.75}Cd_{0.25}Se$/ZnSe QW's and bulk ZnSe. Approximate results for $\Gamma_{\mathrm{LO}}(L_W)$ are also shown (dashed line) for the range 120 Å $\le L_W \le$ 225 Å, though the independent subband approximation is not reliable in this regime and the effects of continuum final states (dissociated electron-hole pairs) have not been included. The theoretical results exhibit structure, to be explained below, which is not confirmed by but is consistent with the limited amount of experimental data. In particular, the theoretical results are consistent with the experimental observations of Pelekanos *et al.*[10] that Γ_{LO} has a value smaller than that of bulk ZnSe for narrow QW's [Γ_{LO}(30 Å)=25 meV and Γ_{LO}=60 meV for bulk ZnSe] and a larger value for wide QW's [Γ_{LO}(200 Å)=90 meV]. This point is emphasized by the arrows in Fig. 2.

This behavior, as explained in detail below, results from a density-of-states argument: the number of scattering states is smaller for narrow QW's than for bulk material and greater than bulk material for wide QW's. In the 30-Å QW's the exciton binding energy E_B exceeds $\hbar\omega_{\mathrm{LO}}$, and single LO-phonon absorption cannot dissociate the exciton into the electron-hole continuum, but only scatter it into other bound 1s exciton states associated with HH1-$C1$. In the 200-Å well E_B is smaller, and energy-conserving scattering states include both bound and continuum excitons associated with HH1-$C1$. Further, the intersubband spacing decreases with L_W so that states associated with other subband pairs, such as HH2-$C1$,[29] are available as well. Note that even without the inclusion of continuum final states, which increase Γ_{LO}, the approximate theoretical value of Γ_{LO} (200 Å) exceeds the value for bulk ZnSe.

Interesting structure, to be discussed below, is obtained near 55 Å, which is weak and due to intra-SL-subband transitions from 1s to 2s and 2p exciton states, and near 100 Å which is strong and due to inter-SL-subband transitions from the 1s HH1-$C1$ exciton to the 1s HH2-$C1$ exciton. This latter structure is replicated with the entry of each new subband pair which are, in order of increasing well width of appearance, HH3-$C1$, HH1-$C2$, and HH4-$C1$. Note that the size of the discontinuous steps associated with transitions to HHn-$C1$ and HH1-Cn states fall off for large n as n^{-2}. The independent subband approximation breaks down as other subbands enter. A correct calculation in the wide-well regime would yield a broad peak subsuming the sharp structure which would decay asymptotically to the value characteristic of bulk excitons (60 meV) for wells significantly wider than 200 Å. Such a calculation is technically far more difficult and will not be discussed here.

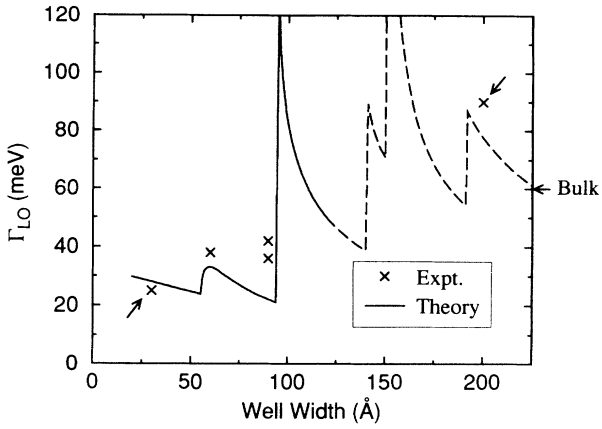

FIG. 2. Calculated homogeneous linewidth Γ_{LO} as a function of well width (solid curve) and experimentally determined values (crosses) from Refs. 10 and 24 for $Zn_{0.75}Cd_{0.25}Se$/ZnSe quantum wells. Also shown at right is the experimental value Γ_{LO}=60 meV for bulk ZnSe (Ref. 10). Calculated results are shown as a dashed line for well widths greater than 120 Å, where the approximations employed are only qualitatively valid. Arrows emphasize experimental points (Ref. 10) showing that Γ_{LO} is smaller and larger than in bulk ZnSe for narrow and wide quantum wells, respectively.

To illustrate the origin of these features, Fig. 3 shows the exciton band structures associated with HH1-$C1$ and HH2-$C1$. Figures 3(a) and 3(b), characteristic of narrow 60–90-Å well widths, are sketched on a *common* energy scale defined with respect to the "vacuum" or ground state containing no excitons. E_1^* and E_2^* are the excitation energies associated with the 1s excitons corresponding to HH1-$C1$ and HH2-$C1$, respectively. E_1^B and E_2^B are the binding energies of these excitons relative to their respective continuum band edges. The arrows in Fig. 3(a) connecting the $\mathbf{K}=\mathbf{0}$, HH1-$C1$ 1s state and the $\mathbf{K}\neq\mathbf{0}$ 1s and 2s/2p states represent phonon absorption processes. Note, by referring to the energetic positions of features in Figs. 3(a) and 3(b), that while the HH1-$C1$ exciton band shown does permit transitions to 2s/2p states, transitions to HH2-$C1$ states are not possible because $\hbar\omega_{\mathrm{LO}}$, indicated in the figure, is too small.

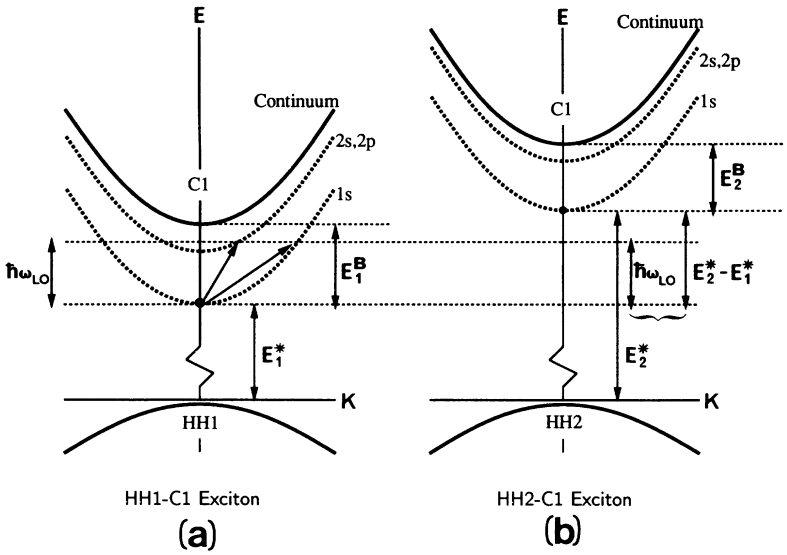

FIG. 3. Schematic illustration of the LO-phonon scattering of the HH1-$C1$ $1s$ $K=0$ exciton showing (a) HH1-C1 and (b) HH2-$C1$ final states typical of well widths in the range 60–90 Å; single-tipped arrows in (a) indicate transitions to $K\neq 0$ $1s$ and to $2s/2p$ states. For narrower wells the exciton binding energy E_1^B increases, and $2s/2p$ states are not accessible. For broader wells the relative sizes of $E_2^*-E_1^*$ and $\hbar\omega_{LO}$ [curly bracket in (b)] interchange, and scattering to the HH2-$C1$ exciton becomes possible.

As shown in Fig. 2, $\Gamma_{LO}(30\text{ Å})$ is smaller than the Γ_{LO} values for the other QW's and the bulk material as emphasized by the arrow in the figure. This is because the 30-Å QW HH1-$C1$ exciton binding energy E_1^B turns out to be sufficiently larger than $\hbar\omega_{LO}$ that only the $\mathbf{K}\neq 0$ $1s$ HH1-$C1$ excitons are possible final states. The fact that no continuum final states are available accounts for the decrease in Γ_{LO} from its bulk value.

The feature in the theoretical curve of Fig. 2 near $L_W=60$ Å is due to transitions to $2p$ final states (the coupling to the $2s$ final states is much smaller). As L_W increases from 30 Å, E_1^B becomes smaller. When $\hbar\omega_{LO}=E^*_{2s,2p}-E_1^*$, where $E^*_{2s,2p}$ is the excitation energy of that exciton at $K=0$, the HH1-$C1$ $2s$ and $2p$ final states become accessible. This occurs at $L_{W,0}\approx 55$ Å and brings about the situation illustrated by the arrow connecting $1s$ to $2s,2p$ states in Fig. 3(a) which applies to well widths greater than $L_{W,0}=55$ Å. The difference between the $1s$ and $2s/2p$ exciton binding energies is a smooth function of well width (see Fig. 1 of Ref. 5). To a good approximation $E^*_{2s,2p}-E_1^*\approx\hbar\omega_{LO}-(2.0\text{ meV/Å})\times(L_W-L_{W,0})$ over the range $55\text{ Å}<L_W<70$ Å. Conservation of energy requires $\hbar^2K^2_{2s,2p}/2M_{HH1,C1}=\hbar\omega_{LO}-(E^*_{2s,2p}-E_1^*)$, and hence $K_{2s,2p}\propto(L_W-L_{W,0})^{1/2}$. For small $K_{2s,2p}$, I_{2s} and I_{2p} of Eq. (10) both vanish with K, but since $I_{2s}(K)$ goes as K^2 and $I_{2p}(K)$ goes as K, transitions to $2p$ final states dominate. The integral $J_1(K)$ defined by Eq. (9) has a limiting value of unity for $K=0$. Hence the contribution to Γ_{LO} from the $2p$ final states varies as $K_{2p}\propto(L_W-L_{W,0})^{1/2}$, giving rise to the discontinuity in the slope of $\Gamma_{LO}(L_W)$ at $L_{W,0}$.

The discontinuous jump in Γ_{LO} in Fig. 2 near $L_W=95$ Å is due to transitions to HH2-$C1$ $1s$ exciton states [cf. Fig. 3(b)]. In addition to decreasing the exciton binding energies, increasing L_W also decreases the valence-subband separations. In particular, at $L_{W,1}\approx 95$ Å the gap between HH2 and HH1 becomes small enough that the exciton energy of the $1s$ HH2-$C1$ exciton E_2^* lies just $\hbar\omega_{LO}$ above E_1^*. At this point transitions to HH2-$C1$ excitons become possible. The curly bracket in Fig. 3(b) illustrates the case for $L_W<95$ Å when $E_2^*-E_1^*$ is larger than $\hbar\omega_{LO}$. Unlike the $J_1(K)$ integral, the $J_2(K)$ integral corresponding to HH2-$C1$ transitions vanishes linearly with K. By contrast, the I_{1s} integral now approaches a finite value. Thus, Γ_{LO} has a large *discontinuous* jump when $\hbar\omega_{LO}=E_2^*-E_1^*$. The K_f^{-1} factor in Eq. (8) arising from the electron-phonon interaction results in a large value of Γ_{LO} when $I_f(0)\neq 0$, since LO-phonon absorption can occur with small in-plane momentum transfer. This factor accounts for the large peak value of Γ_{LO}.

Similar structures associated with the intersubband transitions are seen at 140, 155, and 190 Å, and correspond to the $1s$ exciton states of HH3-$C1$, HH1-$C2$, and HH4-$C1$, respectively. In addition, when $\hbar\omega_{LO}$ begins to exceed E_1^B, which is estimated to occur near $L_W\approx 120$ Å, Γ_{LO} increases as the electron-hole continuum states contribute increasingly to the exciton scattering. As a result, the calculations indicate that a 200-Å QW should exhibit a Γ_{LO} significantly larger than the bulk value, as is experimentally observed and emphasized by an arrow in Fig. 2. This result is clear even though the sharp structure associated with the independent subband approximation in the vicinity of $L_W=200$ Å is expected to be replaced by a broad peak.

The deviations from bulk behavior exhibited by narrow and wide QW's in the $Zn_{1-x}Cd_xSe/ZnSe$ system are thus qualitatively explained. Further, the consistency of the presently existing experimental data with the calculated behavior of Γ_{LO} invites further explorations to verify the interesting theoretically predicted features of $\Gamma_{LO}(L_W)$ just discussed.

ACKNOWLEDGMENTS

We are grateful to A. V. Nurmikko and J. Ding for helpful discussions and for making their data available prior to publication. This work is supported by an ARPA/URI subcontract through Brown University No. 283-25040, the U.S. Joint Services Electronics Program (JSEP) through U.S. Office of Naval Research (ONR)

Contract No. N00014-89-J-1023, and by the U.S. Advanced Research Projects Agency (ARPA) through Contract Nos. N00014-86-K-0033 and N00014-93-1-0549.

APPENDIX

The band structure for $Zn_{1-x}Cd_xSe/ZnSe$ QW's is calculated using a previously developed approach in which the eight-band Kane $\mathbf{k}\cdot\mathbf{p}$ model is used to determine the $\mathbf{K}=\mathbf{0}$ or zone-center states of the heterostructure in terms of products of bulk $\mathbf{k}=\mathbf{0}$ states and envelope functions.[6] Here $\mathbf{K}$ refers to the crystal momentum of a perfectly periodic SL, while $\mathbf{k}$ refers to the bulk constituent semiconductors. The $\mathbf{K}=\mathbf{0}$ states are in turn used as a basis for SL $\mathbf{K}\cdot\mathbf{p}$ theory[7,8] to determine states for $\mathbf{K}\neq\mathbf{0}$, denoted $|L,\mathbf{K}\rangle$, where L is the heterostructure band index. The required input involves only a Kane model parametrization of the bulk constituents and a value for the valence-band offset.

In the $Zn_{1-x}Cd_xSe/ZnSe$ system the lattice mismatch (6.4% between CdSe and ZnSe) results in strain effects which alter the Kane $\mathbf{k}\cdot\mathbf{p}$ Hamiltonian.[30] The strain in the two types of layers in the heterostructure, A and B, can be expressed as a sum of hydrostatic strain

$$e_H^{A(B)}=2\left[1-\frac{C_{12}^{A(B)}}{C_{11}^{A(B)}}\right]e_{\parallel}^{A(B)}, \tag{A1}$$

and biaxial strain

$$e_B^{A(B)}=\left[1+2\frac{C_{12}^{A(B)}}{C_{11}^{A(B)}}\right]e_{\parallel}^{A(B)}, \tag{A2}$$

where $C_{11}^{A(B)}$ and $C_{12}^{A(B)}$ are the elastic stiffness constants and

$$e_{\parallel}^{A(B)}=(a_{\parallel}-a_{A(B)})/a_{\parallel} \tag{A3}$$

is the in-plane strain in each layer; a_A and a_B are the bulk lattice constants. The in-plane lattice constant of the heterostructure, $a_{\parallel}$, is determined by either the substrate or the minimization of the total elastic energy[31] depending upon whether the structure is lattice matched to the substrate or free standing, respectively. This strain results in an additional term in the eight-band bulk $\mathbf{k}\cdot\mathbf{p}$ Hamiltonian which can be expressed as two four-by-four blocks in a basis of Γ_6 conduction (C), Γ_8 light hole (LH) and heavy hole (HH), and Γ_7 split-off (SO) states:

$$\delta H^{A(B)}=\begin{bmatrix} e_H^{A(B)}c^{A(B)} & 0 & 0 & 0 \\ 0 & -e_B^{A(B)}b^{A(B)} & 0 & \sqrt{2}e_B^{A(B)}b^{A(B)} \\ 0 & 0 & +e_B^{A(B)}b^{A(B)} & 0 \\ 0 & \sqrt{2}e_B^{A(B)}b^{A(B)} & 0 & 0 \end{bmatrix} \begin{matrix} (C) \\ (LH) \\ (HH) \\ (SO), \end{matrix} \tag{A4}$$

where $c^{A(B)}$ and $b^{A(B)}$ are the hydrostatic and biaxial deformation potentials, respectively.[32] The valence-band edges have been assumed to be explicitly independent of hydrostatic strain: any strain dependence is assumed to be included in the valence-band offset. This strain Hamiltonian is an additional term in the equation determining the heterostructure envelope functions (Table II of Ref. 7) and its effect is to shift the $\mathbf{k}=\mathbf{0}$ energy levels. The most important effect is the splitting of the Γ_8 degeneracy of the heavy and light holes at the zone center.

The shifts in the Γ_8 energy level and heavy-hole valence-band offset Λ_{HH} which determine the heavy-hole states are

$$E_{\Gamma_8}^{A(B)}\rightarrow E_{\Gamma_8}^{A(B)}+e_B^{A(B)}b^{A(B)} \tag{A5}$$

and

$$\Lambda_{HH}=\Lambda+e_B^A b^A-e_B^B b^B, \tag{A6}$$

where Λ is the offset in the absence of biaxial strain. To second order in the strain the shifts in the Γ_6, Γ_8, and Γ_7 energy levels relevant to the conduction and light-hole states and the light-hole valence-band offset Λ_{LH} are

$$E_{\Gamma_6}^{A(B)}\rightarrow E_{\Gamma_6}^{A(B)}+e_H^{A(B)}c^{A(B)},$$

$$E_{\Gamma_8}^{A(B)}\rightarrow E_{\Gamma_8}^{A(B)}-e_B^{A(B)}b^{A(B)}+2(e_B^{A(B)}b^{A(B)})^2/\Delta^{A(B)},$$

$$E_{\Gamma_7}^{A(B)}\rightarrow E_{\Gamma_7}^{A(B)}-2(e_B^{A(B)}b^{A(B)})^2/\Delta^{A(B)}, \tag{A7}$$

and

$$\Lambda_{LH}=\Lambda-e_B^A b^A+e_B^B b^B+2(e_B^A b^A)^2/\Delta^2-2(e_B^B b^B)^2/\Delta^B, \tag{A8}$$

where $\Delta^{A(B)}$ is the spin-orbit splitting in the absence of strain. In $Zn_{1-x}Cd_xSe/ZnSe$ QW's the $Zn_{1-x}Cd_xSe$ well layers are under biaxial compression. Thus the heavy-hole edge is higher in energy than the light-hole edge. As a result Λ_{HH} is larger than Λ_{LH}, and heavy-hole states are confined by a higher effective barrier than the light-hole states.

[1]M. A. Haase, J. Qui, J. M. DePuydt, and H. Cheng, Appl. Phys. Lett. **59**, 1272 (1991).

[2]H. Jeon, J. Ding, W. Patterson, A. V. Nurmikko, W. Xie, D. C. Grillo, M. Kobayashi, and R. L. Gunshor, Appl. Phys. Lett. **59**, 3619 (1991).

[3]N. F. Johnson, J. Phys. Condens. Matter **2**, 2099 (1990).

[4]P. M. Young, P. M. Hui, and H. Ehrenreich, Phys. Rev. B **44**, 12 969 (1991).

[1]M. A. Haase, J. Qui, J. M. DePuydt, and H. Cheng, Appl. Phys. Lett. **59**, 1272 (1991).
[2]H. Jeon, J. Ding, W. Patterson, A. V. Nurmikko, W. Xie, D. C. Grillo, M. Kobayashi, and R. L. Gunshor, Appl. Phys. Lett. **59**, 3619 (1991).
[3]N. F. Johnson, J. Phys. Condens. Matter **2**, 2099 (1990).
[4]P. M. Young, P. M. Hui, and H. Ehrenreich, Phys. Rev. B **44**, 12 969 (1991).
[5]P. M. Young, H. Ehrenreich, P. M. Hui, and N. F. Johnson, J. Appl. Phys. **74**, 7369 (1993).
[6]N. F. Johnson, H. Ehrenreich, K. C. Hass, and T. C. McGill, Phys. Rev. Lett. **59**, 2352 (1987).
[7]N. F. Johnson, H. Ehrenreich, P. M. Hui, and P. M. Young, Phys. Rev. B **41**, 3655 (1990).
[8]P. M. Young, Ph.D. thesis, Harvard University, 1992.
[9]J. Ding and A. V. Nurmikko (unpublished).
[10]N. T. Pelekanos, J. Ding, M. Hagerott, A. V. Nurmikko, H. Lou, N. Samarth, and J. L. Furdyna, Phys. Rev. B **45**, 6037 (1992).
[11]J. Ding, H. Jeon, T. Ishihara, M. Hagerott, A. V. Nurmikko, H. Luo, N. Samarth, and J. Furdyna, Phys. Rev. Lett. **69**, 1707 (1992).
[12]P. M. Young and H. Ehrenreich, Appl. Phys. Lett. **61**, 1069 (1992).
[13]J. Ding, N. Pelekanos, A. V. Nurmikko, H. Luo, N. Samarth, and J. K. Furdyna, Appl. Phys. Lett. **57**, 2885 (1990).
[14]N. Samarth, H. Luo, J. K. Furdyna, R. G. Alonso, Y. R. Lee, A. K. Ramdas, S. B. Qadri, and N. Otsuka, Appl. Phys. Lett. **56**, 1163 (1990).
[15]P. Lawaetz, Phys. Rev. B **4**, 3460 (1971).
[16]B. Sermage and G. Fishman, Phys. Rev. B **23**, 5107 (1981).
[17]H. W. Hölscher, A. Nöthe, and Ch. Uihlein, Phys. Rev. B **31**, 2379 (1985).
[18]N. Samarth, H. Luo, J. K. Furdyna, S. B. Qadri, Y. R. Lee, A. K. Ramdas, and N. Otsuka, Appl. Phys. Lett. **54**, 2680 (1989).
[19]B. H. Lee, J. Appl. Phys. **41**, 2984 (1970).
[20]R. M. Martin, Phys. Rev. B **6**, 4546 (1972).
[21]A. Blancha, H. Presting, and M. Cardona, Phys. Status Solidi B 126, 11 (1984).
[22]G. E. Hite, D. T. F. Marple, M. Aven, and B. Segall, Phys. Rev. **156**, 850 (1967).
[23]The valence-band hydrostatic deformation potential employed in Ref. 10 implies that Λ would be negative if strain were the only source of the offset.
[24]J. Ding, M. Hagerott, T. Ishihara, H. Jeon, and A. V. Nurmikko, Phys. Rev. B **47**, 10 528 (1993).
[25]Acoustic-phonon scattering is estimated to contribute less than 2 meV to the linewidth. See J. Lee, E. Koteles, and M. O. Vassell, Phys. Rev. B **33**, 5512 (1986), and the discussion in Ref. 10.
[26]R. Zimmermanm, J. Cryst. Growth **101**, 346 (1990).
[27]Similar calculations for lifetimes of *band* electrons (not excitons) can be found in P. J. Price, Ann. Phys. **133**, 217 (1981), and Ref. 28.
[28]R. Ferreira and G. Bastard, Phys. Rev. B **40**, 1074 (1989).
[29]Note that the HH2-$C1$ exciton does not appear in the optical spectra because it violates the $\Delta n = 0$ selection rule for optical absorption.
[30]P. Voison, in *Third Brazilian School of Semiconductor Physics,* edited by C.E.T. Gonçalves da Silva, L. E. Oliveira, and J. R. Leite (World Scientific, Singapore, 1987), p. 46.
[31]C. Kittel, *Introduction to Solid State Physics,* 4th ed. (Wiley, New York, 1971), pp. 135–156.
[32]In the chosen sign convention, c and b are typically negative.